

MOL #56598

## **A non-desensitizing kainate receptor point mutant**

Naushaba Nayeem<sup>1</sup>, Yihong Zhang<sup>1,2</sup>, Devin K. Schweppe, Dean R. Madden and Tim Green

Department of Pharmacology, School of Biomedical Sciences, University of Liverpool,  
Liverpool, UK. (N.N., Y.Z. & T.G.); Department of Biochemistry, Dartmouth Medical School,  
Hanover, NH, USA (D.K.S. & D.R.M.)

MOL #56598

**Running title:** Non-desensitizing kainate receptor mutant

Correspondence and proofs to: Tim Green  
address as above  
Tel.: +44 (0)151 794 5564  
Email: tpgreen@liv.ac.uk

Number of text pages: 32  
Number of tables: 2  
Number of figures: 4  
Number of references: 36  
Number of words in *Abstract*: 233  
Number of words in *Introduction*: 496  
Number of words in *Discussion*: 1373

**Abbreviations:**

iGluR, ionotropic glutamate receptor; KA, kainate; AMPA,  $\alpha$ -amino-3-hydroxy-5-methyl-4-isoxazolepropionic acid; HEK, human embryonic kidney; WT, wild type.

MOL #56598

## ABSTRACT

Ionotropic glutamate receptor (iGluR) desensitization can be modulated by mutations that change the stability of a dimer formed by the agonist binding domain. Desensitization of AMPA receptors can be blocked by a single point mutation (e.g. GluR2 L483Y) that stabilizes this dimer in an active conformation. In contrast, desensitization of kainate receptors can be slowed, but not blocked, by similar dimer interface mutations. Only covalent cross-linking via introduced disulfides has been previously shown to block kainate receptor desensitization completely. We have now identified an apparently non-desensitizing GluR6 point-mutant (Asp776 to lysine; D776K), located at the apex of the ligand binding (S1S2) domain dimer interface. Asp776 is one of a cluster of four charged residues in this region, which together mediate direct dimer interactions, and also contribute to the binding sites for one chloride and two sodium ions. Despite the localized +4 change in the net-charge of the S1S2 dimer, the D776K mutation actually increased the thermodynamic stability of the dimer. Unlike GluR6 wild-type, the D776K mutant is insensitive to external cations, while retaining sensitivity to external anions. We therefore hypothesize that the unexpected phenotype of this charge-reversal mutation results from the substitution of the sodium ions bound within the dimer interface by the introduced lysine  $\text{NH}_3^+$  groups. The non-desensitizing D776K mutant provides insights into kainate receptor gating, as well as representing a potentially useful new tool for dissecting kainate receptor function.

MOL #56598

Desensitization, receptor inactivation in the continued presence of agonist, has a profound influence on the magnitude and duration of kainate- and AMPA-selective iGluR responses. Following activation by the endogenous agonist glutamate (Glu), desensitization is generally rapid (time constants typically ~1-10 ms) and substantially complete (96-99.7%) (Dingledine et al., 1999; Ozawa et al., 1998). Desensitization is an intrinsic property of the receptor subunits themselves, and is therefore an integral part of the overall gating mechanism of these receptors.

Functionally, desensitization occurs independently of channel opening. As tetramers, iGluRs can bind up to four agonist molecules; agonist binding to at least two subunits is required to drive channel gating (Clements et al., 1998; Heckmann et al., 1996; Rosenmund et al., 1998), but agonist binding to one or more subunits is sufficient for entry into desensitized states (Heckmann et al., 1996; Robert and Howe, 2003). Concentrations of agonist too low to activate responses are therefore able to cause desensitization. The process of desensitization is reversible, with agonist responses recovering completely once agonist is removed. The rate of this recovery from desensitization varies significantly between iGluR subtypes, with multiple overlapping time-constants revealing the existence of a number of distinct desensitized states (Robert and Howe, 2003).

From a structural standpoint, our view of the desensitization process comes largely from crystallographic studies of the isolated agonist-binding or “S1S2” domain. Structures of the S1S2 domain have been determined for both AMPA and kainate receptor subunits, revealing a conserved bilobate structure (Gouaux, 2004; Mayer, 2006). In both subtypes S1S2 domains have been observed to form two-fold symmetrical, back-to-back dimers (Armstrong and Gouaux, 2000; Nanao et al., 2005). The stability of the S1S2 dimer has been found to correlate inversely with desensitization rates. In particular, a leucine to tyrosine AMPA-receptor point-mutant,

MOL #56598

which completely blocks desensitization (Stern-Bach et al., 1998), stabilizes the S1S2 dimer by strengthening inter-subunit contacts (Sun et al., 2002). These observations suggest that dimer rearrangement is required for desensitization, an interpretation subsequently corroborated for both AMPA- and kainate-receptor subtypes (Horning and Mayer, 2004; Priel et al., 2006; Weston et al., 2006; Zhang et al., 2006).

Despite the common role of the S1S2 dimer interface, there are also differences between AMPA and kainate receptor desensitization. For one thing, it has proven difficult to suppress desensitization in the kainate receptors by stabilizing purely non-covalent interactions. In addition, in kainate receptors response amplitudes and desensitization rates are dependent on external ions (Bowie, 2002; Paternain et al., 2003). Binding sites have been identified at the apex of the S1S2 dimer for both anions and cations (Plested and Mayer, 2007; Plested et al., 2008), consistent with studies in which mutations in this region affected desensitization rates (Fleck et al., 2003; Wong et al., 2006; Wong et al., 2007). In this study we have characterized the electrophysiological and biochemical consequences of additional apical mutations; in particular the effects on receptor responses of charge-reversal mutations. Their effects highlight the key role of this region as a regulator of receptor desensitization.

## **MATERIALS AND METHODS**

### *Mutagenesis*

All mutagenesis was carried out on a rat GluR6(Q) cDNA clone. Residue numbering is from the start methionine (subtract 31 for GluR6 and 30 for GluR5 to obtain numbering based on predicted mature polypeptide). Mutants were generated using the QuikChange protocol and *Pfu*

MOL #56598

turbo polymerase (Stratagene, La Jolla, CA), essentially as described in Zhang et al. (2006). All mutants were confirmed either by sequencing of the entire open reading frame, or by sequencing after subcloning of the 1.65kb XagI-Eco47III fragment. Crystal structures for GluR6 S1S2-Dom (RCSB protein data bank accession 1YAE) (Nanao et al., 2005) and GluR5 S1S2-KA (accession 3C32) (Plested et al., 2008) were used to generate figures using *MacPyMOL* (<http://pymol.sourceforge.net/>).

### *Cell culture, Electrophysiology & Data Analysis*

HEK-293 cell culture, whole-cell patch clamp and data analysis were carried out as described previously (Zhang et al., 2008). Whole-cell recordings were made 48-72 h after transfection at a holding potential of -70 mV using a HEKA Elektronik EPC 10 amplifier. The electrode solution contained (in mM): 110 CsF, 30 CsCl, 4 NaCl, 0.5 CaCl<sub>2</sub>, 10 HEPES, and 5 EGTA (adjusted to pH 7.3 with CsOH). The external bath solution contained (in mM): 150 NaCl, 2.8 KCl, 1.8 CaCl<sub>2</sub>, 1.0 MgCl<sub>2</sub>, and 10 HEPES (adjusted to pH 7.3 with NaOH). Rapid agonist application was achieved using the Burleigh LSS-3200 piezo-based system. The rate of solution exchange in this system (determined by open-tip junction currents) was <250 μs, and 20-80% rise-times for control (GluR6 WT) responses were <1 ms. Recordings were performed on small-diameter cells (20 μm), lifted into the perfusion stream to ensure rapid solution exchange (Zhang et al., 2008). Time constants were determined using single-exponential fits in *PulseFit* (HEKA). For GluR6 WT, steady-state decay rates were determined from responses with clear steady states (those fitted ranged between 15-75 pA from peak responses of 3-15 nA).

Oocytes were injected with cRNA (~50 nl; 0.8 mg/ml) transcribed from the GluR6 WT and mutant cDNAs (in pcDNA3.1; linearized with Xba I) using the mMessage mMachine T7 kit (Ambion, Warrington, UK). Current recordings were made 48-56 h after injection using the set-

MOL #56598

up described in Thompson & Lummis (2008). The control external medium (in mM: 96 NaCl, 1.1 KCl, 1.8 BaCl<sub>2</sub>, 5 HEPES, adjusted to pH 7.5 with NaOH) was modified by substitution of NaCl with NaF, NaNO<sub>3</sub>, CsCl or RbCl as appropriate. Where the cation was exchanged the pH was adjusted using CsOH instead of NaOH. Recordings were made at a holding potential of -60mV, with agonist (10 mM Glu) applied for 10 s at a flow rate of 10 ml/min. Oocytes expressing GluR6 WT were pre-treated with concanavalin A (0.3 mg/ml, 0.2 µm filtered; incubated for 5-10 min) prior to recording. The program *WCP* (J. Dempster, University of Strathclyde, UK) was used for oocyte data recording and analysis.

All data are presented as mean±S.E.M. Statistical analyses were carried out using *Prism* (v5; GraphPad Software). Significant differences compared to the GluR6 WT control were identified by unpaired t-test for single comparisons and using 1-way ANOVA for multiple comparisons. In the latter case significance was tested using either Dunnett's or Dunn's multiple comparison tests depending on data variances.

### *S1S2 Domain Expression and Characterization*

Overlap-extension PCR was used to generate a GluR6 S1S2 domain construct in the pET21 bacterial expression vector (Novagen, Nottingham, UK). The construct was based on the domain boundaries described by Mayer (2005), and included GluR6 residues Ser429 to Lys544 and Pro667 to Glu806, joined by a GlyThr linker sequence, and ending with a six-histidine tag. This construct was recombinantly expressed (induction with 1 mM IPTG; 4 h, 23°C) in BL21(DE3) cells (Bioline, London, UK). Constructs were purified to homogeneity following chemical lysis (Cellytic-B; Sigma-Aldrich, Poole, UK) in three chromatography steps, using a base buffer containing 150 mM NaCl, 25 mM HEPES, 5% (v/v) glycerol and 1-5 mM glutamate. The steps were; His-select nickel-affinity (Sigma; pH 7.5, elution with 400 mM imidazole), HiTrapQ

MOL #56598

anion-exchange (GE Healthcare, Piscataway, NJ; pH 8.0, sample in flow-through) and Superdex-75 gel filtration (GE Healthcare; pH 7.5). The final yield ranged between 0.2-0.5 mg/L culture.

Purified S1S2 constructs were concentrated by ultra-filtration as required. Blue-Native polyacrylamide gel electrophoresis (BN-PAGE) was carried out using Novex 4-16% NativePAGE gels and associated buffers (Invitrogen, Paisley, UK) according to the manufacturer's instructions. Protein bands were visualized either directly with Coomassie Blue R-250 or silver staining, or following electro-blotting onto Immobilon-P (Millipore, Watford, UK) and detection with an anti-His tag monoclonal antibody (1:1,000 dilution; Sigma).

For size exclusion chromatography and ultracentrifugation, samples were initially concentrated to an  $A_{280}$  of ~0.4-0.6 and then dialyzed into 25mM HEPES, pH 7.5, 150 mM NaCl, 5% (w/v) glycerol, 1 mM sodium glutamate, and 0.02% (w/v)  $\text{NaN}_3$ . Size-exclusion chromatography was performed on a Superdex-75 10/30 column. The WT and D776K proteins each eluted as single peaks, and corresponding  $\ln(\text{MW})$  and Stokes radius estimates were obtained by linear regression analysis of globular standards.

Ultracentrifugation experiments were performed at 20°C in a Beckman ProteomeLab XL-A centrifuge equipped with an AN-60 rotor and absorbance optics. Sedimentation velocity experiments were performed at a rotor speed of 35k rpm. Absorbance scans were taken at 280 nm at ~1.25 minute intervals, with a 0.003 cm radial scan step. Sedimentation equilibrium data were recorded for 10 hours each at speeds of 7k, 10k, 14k, 20k, and 28k rpm. Scans were taken at 1 h intervals with a 0.001 cm step size along the radial axis and 5 replicates/data point. Attainment of sedimentation equilibrium was verified using the program WinMATCH (D.A. Yphantis and J.W. Lary; [www.biotech.uconn.edu/auf](http://www.biotech.uconn.edu/auf)) Six-sector cells were loaded with 1x-, 2x-, and 4x-dilutions of ~10  $\mu\text{M}$  stock solutions. Curves collected at all five speeds for the two highest-



MOL #56598

concentration channels were globally fit. Protein partial specific volume ( $\bar{v}$ ) and buffer density and viscosity ( $\rho$ ,  $\eta$ ) were calculated using the program SEDNTERP (J. Philo, D. Hayes, and T. Laue) (Laue et al., 1992). Sedimentation coefficient distributions were calculated using the program SEDFIT87 (Dam and Schuck, 2004). Sedimentation equilibrium data were analyzed using the program SEDANAL (Stafford and Sherwood, 2004), using both single-species and oligomerization models.

#### *Biotinylation, deglycosylation & radioligand binding*

Cell surface expression was determined following biotinylation as described previously (Zhang et al., 2006) and quantified using Kodak 1D software. Deglycosylation experiments using Endo H and PNGase F (New England Biolabs, Hitchin, UK) were performed essentially as described by Priel et al. (2006). Briefly, membranes were prepared from cells 55-60 h following transient transfection with full-length GluR6 constructs, and membrane aliquots containing 20  $\mu$ g of total protein incubated with 1  $\mu$ l of the enzymes for 2 h at 37°C in the supplied buffers. Immunoblots for both surface labeling and deglycosylation experiments were carried out using polyclonal GluR6/7 antisera (1:1000 dilution; Upstate, Chandlers Ford, UK).

For radioligand binding assays, membrane preparations and [ $^3$ H]kainate saturation and displacement assays were performed as described previously (Zhang et al., 2006), using membrane preparations from HEK cells stably expressing GluR6 D776K (following G418 selection). Data were fitted by non-linear regression using built-in functions in *Prism*.

MOL #56598

## RESULTS

We had previously used a combination of site-directed mutagenesis and whole-cell patch clamp in HEK-293 cells to identify GluR6 S1S2 domain mutations that slowed desensitization kinetics (Zhang et al., 2006). The residues in that study were clustered around Tyr521, the homolog of the non-desensitizing GluR2 L483Y mutant. Inter-subunit interactions in this region play an important role in determining dimer stability and therefore desensitization rates. A second point of contact in S1S2 dimers is evident in crystal structures (Fig. 1A) (Armstrong and Gouaux, 2000; Nanao et al., 2005). This comprises either a pair (in AMPA receptor subunits) or quartet (in kainate receptor subunits) of charged residues capable of forming inter-subunit salt-bridges at the apex of the dimer. In GluR6, contacts are formed between Glu524 and Lys531, the equivalent of which is also found in AMPA receptor subunits, and between Arg775 and Asp776 (Fig. 1B), an interaction found only in kainate receptor subunits (Nanao et al., 2005). This region is also where a single chloride and two sodium ions bind in kainate receptor subunits (Fig. 1C) (Plested and Mayer, 2007; Plested et al., 2008), complicating any interpretation of how the various charged amino acids interact. Indeed, the GluR5 homolog of Arg775 (Arg790) shows conformational flexibility in the presence of different cations, such that an inter-subunit contact is not always formed (Plested et al., 2008).

### **Switching charges at the S1S2 apex has varied effects on desensitization kinetics**

To better understand the role of these residues in receptor function we determined the effect of single and double charge-exchanges at these four sites. These experiments revealed a spectrum of effects consistent with perturbations of the S1S2 dimer interaction, ranging from loss of response to almost complete block of desensitization (Fig. 2, Table 1). We first assessed the effect of double mutations at the two charge-pairs: Glu524-Lys531 and Arg775-Asp776, in which the

MOL #56598

respective charged amino acids were exchanged. Mutants were transiently transfected into HEK cells, and responses to applications of Glu (3 mM) and KA (1 mM) determined by whole-cell voltage clamp recordings. As their overall effect was charge-neutral, these mutants should reveal the extent to which geometry at these sites, as opposed simply to charge, is important in receptor function. The E524K-K531E mutant was still functional, but with responses to Glu and KA that desensitized 3- to 4-fold faster than those of GluR6 WT (Fig. 2A, Table 1). For the R775D-D776R mutant, in contrast, no responses were observed with either agonist (Table 1). This indicates that the environment in the vicinity of Arg775 and Asp776 is more sensitive to changes in charge distribution than that around Glu524 and Lys531.

We next mutated these four residues singly to reverse the charge of their sidechains. Given their location and the effect of the double mutants, these single mutants would be expected to destabilize the dimer and therefore attenuate responses. For the E524K and R775D mutations this was indeed the case, with responses either entirely absent (E524K) or extremely small (R775D) (Fig. 2A, Table 1). This was in agreement with the reported effects of other changes to these sites in AMPA and kainate receptor subunits (Fleck et al., 2003; Horning and Mayer, 2004; Plested and Mayer, 2007; Wong et al., 2007). With the K531E mutation, in contrast, desensitization in response to both Glu and KA was actually slowed (Fig. 2A, Table 1). While unexpected, this was again consistent with published data, at least for kainate receptors. In GluR6 the K531G mutation has been found to slow desensitization, particularly in response to KA (Fleck et al., 2003). Similar mutations to the homologous site in GluR2 (*i.e.* K493A & M) accelerated desensitization, as would be predicted (Horning and Mayer, 2004). Our K531E mutation does not resolve the question of why changes to this site have unexpected effects on kainate receptor responses, but it does appear to rule out simple steric effects (Horning and Mayer, 2004).

MOL #56598

### **Replacing Asp776 with a lysine blocks receptor desensitization**

The last of the four charge-reversal mutations we tested, Asp776 to lysine (D776K), would again be expected to severely attenuate or even eliminate receptor responses. This was the effect of other reported mutations at this site in GluR6. Mutation of Asp776 to asparagine, glutamate or glycine accelerated desensitization, while mutation to threonine abolished responses (Fleck et al., 2003; Plested and Mayer, 2007). The D776K mutant had a very different phenotype. While most cells showed no agonist-activated responses, in a minority (30/116) currents were observed. These responses were essentially non-desensitizing to agonist applications up to 4 s, desensitizing by around 10% with both Glu and KA (Fig. 2B & Table 1). Current amplitudes varied greatly for responses to both Glu (range 11 pA to 5.5 nA, mean 830 pA, median 262 pA) and KA (range 9 pA to 4.7 nA, mean 810 pA, median 270 pA). Consistent with the absence of desensitization, repeated 100 ms applications in a paired-pulse protocol showed no sign of desensitization or appreciable run-down (n=6; data not shown). While only 25% of transiently-transfected cells gave currents for D776K, later tests on HEK cells stably-transfected with D776K showed smaller but more reliable responses to Glu (22/52 responded; range 13-620 pA, mean 156 pA, median 61 pA). Unless otherwise indicated, the characterization of D776K described below was carried out using transiently-transfected cells.

Comparing agonist efficacy between GluR6 WT and D776K, the overall rank order of efficacy for Glu, KA and domoate (another partial agonist) was maintained (Glu > KA > domoate). The relative efficacy of KA was slightly higher in D776K (Table 1), but there was no difference in the relative efficacy of domoate (100  $\mu$ M) between GluR6 WT ( $0.33 \pm 0.03$ , n=6) and D776K ( $0.35 \pm 0.03$ , n=14). Comparing D776K currents in response to Glu and KA, their rise times were similar at  $\sim 4$  ms &  $\sim 3$  ms respectively (compared to  $< 1$  ms for WT and other constructs), as were

MOL #56598

their desensitization kinetics (for the ~10% of the D776K response that desensitized, the kinetics were poorly fitted by exponential decays, but time-constants were around 1-2 seconds).

Where the responses to the two agonists differed was in their decay rates from peak responses (Fig. 2C). The decay rates from brief (1 ms) agonist applications were determined for GluR6 WT and D776K. Deactivation rates from peak responses to Glu were unaffected by the mutation, whereas deactivation rates from peak responses to KA were slowed over 10-fold in D776K compared to GluR6 WT (Fig. 2C & Table 2). A similar agonist-selective effect on decay was not apparent with decay rates from steady state responses ( $\tau_{Dec-SS}$ ). For both agonists  $\tau_{Dec-SS}$  was higher than  $\tau_{Dec-1ms}$ , but this was true for GluR6 WT as well as D776K (Table 2). In the non-desensitizing GluR1 mutant L497Y the deactivation rate from peak responses is slowed, whereas the modulator cyclothiazide blocks desensitization without affecting deactivation rates (Mitchell and Fleck, 2007). Therefore, at least in terms of deactivation rates, KA-induced D776K responses behave similarly to those of GluR1 L497Y (slower deactivation), whereas Glu-induced D776K responses are more akin to cyclothiazide-treated GluR1 (normal deactivation). In very general terms this implies differences in the stability of receptor states when Glu and KA are bound (see *Discussion*).

### **Increased dimer stability in GluR6 D776K**

It is clear from studies in GluR2 that AMPA-receptor desensitization is inversely correlated with the stability of the dimer formed between S1S2 domains. While the S1S2 domain of GluR2 WT shows only a very weak tendency to dimerize ( $K_d \approx 6$  mM), the GluR2 L483Y mutant dimerizes with a dissociation constant of 30 nM (Sun et al., 2002). We therefore investigated the tendency of the D776K S1S2 domain to dimerize in comparison with GluR6 WT. S1S2 domains were

MOL #56598

recombinantly expressed and purified as described in the *Material and Methods*, and their aggregation state assessed by gel filtration, blue-native gel electrophoresis (BN-PAGE) and analytical ultracentrifugation.

Gel filtration experiments indicated a higher apparent molecular weight, with a clear difference in retention time for D776K compared to GluR6 WT (Fig. 3A). When the retention times were calibrated against globular standards, the relative molar mass ( $M_r$ ) of the WT protein was estimated as 31 kDa, compared to 50 kDa for the D776K mutant. The calculated value for both proteins is 32 kDa. To test the possibility that the altered mutant retention time was caused by a change in hydrodynamic radius (e.g. elongation), sedimentation coefficients were determined for both wild-type and mutant proteins in velocity sedimentation experiments, and the gel-filtration data were re-calibrated in terms of Stokes radius. The shape-independent  $M_r$  values obtained from the Svedberg equation were 30 kDa for WT and 56 kDa for the D776K mutant, confirming the increase in average molar mass of the mutant vs. WT S1S2 domains. The  $M_r$  values estimated for the D776K mutant are intermediate between the calculated values for monomeric and dimeric species, consistent with the possibility of an equilibrium among oligomeric species, with an exchange rate faster than the time-scale (hours) of the gel-filtration and sedimentation experiments. This possibility was confirmed by BN-PAGE. While the GluR6 WT was largely ( $81 \pm 7\%$ ,  $n=3$ ) monomeric at the concentrations used ( $\sim 30 \mu\text{M}$  protein stock), a significant proportion ( $47 \pm 6\%$ ,  $n=3$ ) of the D776K mutant ran as a dimer (Fig. 3A). There were also higher-order associations evident for D776K (representing  $5 \pm 2\%$ ,  $n=3$ ); there is however no structural or biochemical evidence that S1S2 domains associate as trimers or tetramers, so it is unlikely that these larger species have a physiological significance.

To further test this model and to quantify the affinity of potential oligomerization interactions, we performed equilibrium analytical ultracentrifugation (AUC) experiments (Fig. 3B). The

MOL #56598

absorbance curves obtained for the GluR6 WT S1S2 could be globally well fit as a single-species, with a molecular weight fixed at the calculated value of 32,214. A representative curve obtained at 14,000 rpm is shown with the associated fit and residuals in Figure 3B (left-hand curves). If a monomer:dimer equilibrium was fitted instead, error analysis showed that the dimerization affinity could not be distinguished from  $K_{eq} = 0$  at the 95% confidence level.

In contrast to the WT protein, a very poor fit was obtained when the equivalent set of D776K S1S2 absorbance curves were fitted with a fixed molecular-weight, single-species model (Fig. 3B; right-hand curves, dashed line & open-circle residuals). However, if a monomer:dimer equilibrium was fitted, a significant improvement was obtained in the quality of fit (Fig. 3B; right-hand curves, solid line & filled-square residuals). The  $K_d$  of dimerization refined to a value of 0.9  $\mu\text{M}$  (95% CI: 0.4-1.4  $\mu\text{M}$ ). The most parsimonious explanation for the hydrodynamic data is that the WT GluR6 S1S2 domain dimerizes only weakly, consistent with previously reported estimates of  $> 8 \text{ mM}$  for the WT  $K_d$  (Chaudhry et al., 2009), and that the D776K mutation stabilizes the dimerization interaction by more than three orders of magnitude.

Desensitization block and dimer stability have also been shown to affect receptor maturation and trafficking (Penn et al., 2008; Priel et al., 2006). The relatively high non-response rate for HEK cells transiently-transfected with D776K implies that expression and/or trafficking are affected by this mutation. This was confirmed by biotin-labeling and immunoblotting (Fig. 3C), which showed very low total and surface expression of D776K compared to GluR6 WT and other constructs, including mutants with very small responses (e.g. E524K, Fig. 3C and R775D, data not shown). Quantification of these immunoblots showed that total levels of both E524K and D776K were about a quarter of GluR6 WT levels ( $24 \pm 7\%$  and  $23 \pm 6\%$  respectively). As a fraction of total levels, surface expression of E524K was not significantly different from GluR6 WT. The fraction of total D776K expressed at the surface, however, was less than half that of GluR6 WT

MOL #56598

( $0.44 \pm 0.19$ ;  $n=5$ ,  $P < 0.05$ ), suggesting a specific trafficking defect associated with the D776K mutation. We also determined ligand affinity (by radioligand binding assay) as a proxy for correct folding. Specific binding of [ $^3$ H]kainate in transiently-transfected HEK cells was too low to allow determination of kainate and glutamate binding affinities. HEK cells stably expressing D776K were therefore used to determine affinity constants. The affinity of kainate for D776K was not significantly different from that for GluR6 WT ( $K_d=12.9 \pm 1.7$  nM,  $n=4$  and  $9.0 \pm 1.9$  nM,  $n=3$  respectively;  $P=0.18$ ). The apparent affinity of Glu was also unchanged in D776K ( $K_i=390 \pm 68$  nM,  $n=3$ ) compared to GluR6 WT ( $K_i=280 \pm 7$  nM,  $n=3$ ;  $P=0.21$ ).

In a final assay, we used the maturation state of receptor glycosylation as an indicator of intracellular localization (Greger et al., 2003; Priel et al., 2006). Membranes isolated from cells transfected with GluR6 WT and D776K were digested using Endo H and PNGase F (Fig. 3D). Endo H only cleaves immature glycosylation added in the endoplasmic reticulum (ER), while PNGase F also removes sugar moieties following maturation in the Golgi. While most GluR6 WT glycosylation was resistant to Endo H treatment ( $78.4 \pm 4.1\%$ ,  $n=4$ ), this percentage was much lower for D776K ( $6.6 \pm 1.5\%$ ,  $n=4$ ). No mature glycosylation was detectable with D776K. It is possible that constitutive activation of D776K leads to cytotoxicity, selecting against cells expressing high receptor levels. In order to counter this we added the non-selective iGluR antagonist CNQX ( $10 \mu\text{M}$ ) to the culture medium, and characterized the resulting responses and glycosylation patterns of D776K. The proportion of non-responding cells treated with CNQX (19/27) was not significantly lower than for non-treated cells (67/89;  $P=0.62$ , Chi squared test). There were also no significant differences in the response sizes, relative agonist efficacies or response kinetics for the two groups. The addition of CNQX to the culture media also had no effect on the glycosylation pattern observed for D776K. In particular, the percentage of receptor resistant to Endo H treatment was unchanged ( $7.6 \pm 1.4\%$ ,  $n=4$ ).



MOL #56598

### **The effect of external cations is abolished by D776K mutation**

Residue Asp776 sits between the anion and cation binding sites located within the dimer interface (Fig. 1C). We therefore investigated whether the D776K mutant affected the sensitivity of the receptor to ions. Current responses of GluR6 WT to glutamate are attenuated and desensitization rates are increased if sodium or chloride ions in the external solution are replaced by other monovalent ions (Bowie, 2002; Paternain et al., 2003). We determined the response amplitude of D776K expressed in *Xenopus* oocytes in various external solutions; replacing sodium ions with either rubidium or cesium ions, and chloride ions with either nitrate or fluoride ions. When the external anion was replaced with either  $\text{NO}_3^-$  or  $\text{F}^-$ , D776K responses were significantly attenuated (to 1-2% of control values; Fig. 4). In contrast, exchanging the external cation for either  $\text{Rb}^+$  or  $\text{Cs}^+$  resulted in responses that were over 30% larger than those in the NaCl control (Fig. 4).

Direct comparison with GluR6 WT responses was not possible in oocytes, but we tested responses following treatment with concanavalin A (ConA) to increase the size of steady-state responses (Fig. 4). As expected, exchange of either cations or anions attenuated GluR6 WT responses in ConA-treated oocytes (responses relative to NaCl control were:  $\text{Rb}^+$ ,  $17 \pm 2\%$ ;  $\text{Cs}^+$ ,  $17 \pm 7\%$ ;  $\text{NO}_3^-$ ,  $3.4 \pm 0.2\%$ ;  $\text{F}^-$ ,  $1.0 \pm 0.7\%$ ;  $n=3-5$ ). The cation effects were similar to those observed in HEK cells ( $\text{Rb}^+$ , 29%;  $\text{Cs}^+$ , 6%) (Plested et al., 2008). The anion effects were larger than those reported in HEK cells ( $\text{NO}_3^-$ , 75%;  $\text{F}^-$ , 14%) (Plested and Mayer, 2007), which may be a consequence of ConA treatment. As noted above, D776K responses were significantly larger than control in both rubidium and cesium (Fig. 4), but the permeability of both ions in GluR6 has been reported to be ~25% higher than that of sodium (Jatzke et al., 2002). We confirmed that this was the most likely explanation for the larger currents by determining slope-conductance responses at

MOL #56598

positive potentials. Outward currents were not significantly higher in the presence of external cesium or rubidium ions compared with the sodium ion control (data not shown).

## DISCUSSION

We investigated the effects on agonist responses of reversing the charges at four sites in the apex of the GluR6 S1S2 agonist binding domain. There are several key inter-subunit contacts in this region, including salt bridges and binding sites for an anion and two cations (Fig. 1). The ion binding sites and one of the two charge-pairs are unique to kainate-selective receptors. Given the proposed importance of dimer interface stability to activation and desensitization, changes that perturb either the charge distribution or the net-charge balance in this region would be expected to significantly accelerate desensitization. Among the single mutants at these four sites, E524K and R775D both attenuated responses as expected (Fig. 2A, Table 1). The other two charge-reversal mutations, K531E and D776K, both had unexpected phenotypes, with desensitization respectively slowed and blocked (Fig. 2A & B). In the case of K531E the effect was relatively small, with an increase in  $\tau_{Des}$  of less than 2-fold for responses to Glu and ~9-fold for responses to KA (Table 1). It was not, however, entirely unexpected, as mutation of Lys531 to glycine also slows desensitization of GluR6 (Fleck et al., 2003). For neither of these mutants does the location of Lys531 in the dimer interface, or the interactions it makes, provide an easy explanation for these phenotypes. This is especially true for K531E, which results in a change in net charge of minus 4 at the dimer apex relative to GluR6 WT. Clearly, an explanation for these phenotypes will require further investigation of the conformations adopted by the S1S2 domain dimer during both receptor activation and desensitization.

MOL #56598

The second single mutant with an unexpected phenotype, D776K, resulted in apparently non-desensitizing responses. This was in marked contrast to the effects of other published mutations at this site, with conservative changes to asparagine and glutamate accelerating desensitization as would be expected (Plested and Mayer, 2007). Elevated steady-state iGluR responses can result either from changes in the relative stability or kinetic accessibility of the desensitized state (e.g. GluR2 L483Y; Sun et al., 2002), or from changes to the relative contributions of different open states (e.g. Concanavalin A; Bowie et al., 2003). While we cannot directly distinguish between these possibilities, we believe the non-desensitizing phenotype of D776K can be explained primarily in terms of S1S2 dimer stability, and therefore desensitization block. First, our biophysical data confirm that, at least in the isolated S1S2 domain, the dimer is clearly stabilized by the D776K mutation. While native gel electrophoresis showed that the GluR6 WT S1S2 domain does associate to a limited extent as a dimer, AUC data indicated that the affinity is very low, consistent with previous reports (Chaudhry et al., 2009; Weston et al., 2006). In contrast, the apparent affinity of the S1S2 dimer interaction was increased >1000-fold by the D776K mutation (Fig. 3B).

A recent study identified a number of GluR6 S1S2 mutations that stabilized the dimer interface, but that reduced the extent of desensitization by less than 20% (Chaudhry et al., 2009). It was therefore proposed that the desensitized state is intrinsically more stable in GluR6 than in GluR2. However, the mutants described in that study all exhibited dimerization constants above 20  $\mu$ M, weaker than the 7  $\mu$ M value observed for a GluR2 mutant that reduced desensitization by only 10% (Sun et al., 2002). For GluR2, substantial block of desensitization is observed only for mutants with stronger dimerization affinities of  $\sim$ 1-5  $\mu$ M (26-52% desensitization) and 30 nM for L483Y (8% desensitization). The S1S2 dimer affinity we observed with D776K (0.9  $\mu$ M), while  $\sim$ 30-fold lower than that of GluR2 L483Y, falls within the range of affinities observed for

MOL #56598

strongly non-desensitizing GluR2 mutants. While our data cannot formally exclude a contribution from destabilization of the desensitized state, the effect of the GluR6 D776K mutation suggests that desensitization in AMPA and kainate receptors is similarly sensitive to the strength of the dimer interface.

These experiments demonstrated that the D776K mutant stabilized the dimer, but they still leave the question of how this occurs. The most likely explanation comes from the location of the sodium binding sites in the dimer interface. It is possible to model a lysine in place of Asp776 without clashes. The C $\beta$  atom of the two Asp776 residues is 6-6.2Å from the nearest sodium ion, and the amine group of each of the lysines can be positioned close to the center of the opposing sodium binding site using a common rotamer (data not shown). In contrast to the chloride binding site, where residues from both subunits interact with the ion, the two sodium binding pockets are largely contained within single subunits, with only limited interactions across the dimer interface (Plested et al., 2008). Therefore, were the lysine side chains in D776K to extend to and effectively occupy the opposing cation binding sites as surrogate cations, this would represent additional inter-subunit interactions. These two new contacts could then serve to lock the conformation of the dimer, preventing desensitization. One consequence would be that the lysines would be expected to displace the sodium ions but not necessarily affect the chloride ion, fully consistent with the observed anion and cation effects of D776K (Fig. 4). The D776K mutant was still sensitive to changes in external anions, unlike the non-desensitizing cystine cross-link mutant (Y521C-L783C), which was insensitive to changes in both external cations and anions (Plested and Mayer, 2007; Plested et al., 2008).

We observed two other effects of D776K; on expression levels and on deactivation kinetics. The surface expression and maturation of D776K in HEK cells appeared attenuated. We cannot rule out cytotoxic effects from constitutive leak currents in D776K-expressing cells but, with that

MOL #56598

important caveat, the observed low surface expression of D776K is consistent with other reports. The trafficking efficiency of AMPA receptor subunits has been found to correlate closely with their desensitization properties (Greger et al., 2003; Penn et al., 2008), while it has been proposed that the ability to desensitize is a key checkpoint in kainate receptor trafficking (Priel et al., 2006). The other interesting effect of D776K was on deactivation kinetics. For the non-desensitizing AMPA receptors there is a concomitant slowing of the rate of deactivation (Sun et al., 2002). The GluR2 L483Y phenotype was initially proposed to result from both stabilization of the open state and destabilization of the desensitized state (see Fig. 5 in Sun et al., 2002). The former was confirmed by determining the rate of channel closure for GluR1 L497Y (Pei et al., 2007), while kinetic modeling of the same mutant suggested that both entry into the desensitized state and the rate of ligand dissociation were decreased relative to GluR1 WT (Mitchell and Fleck, 2007). Although this modeling study did not incorporate slower channel closure, it seems probable that a combination of these three factors blocks desensitization and slows deactivation in the AMPA receptor leucine to tyrosine mutants. It is therefore interesting that peak responses to Glu (but not to KA) deactivate as rapidly as GluR6 WT responses (Fig. 2C), in contrast to the slow deactivation of other GluR6 mutants with attenuated desensitization rates (Chaudhry et al., 2009; Zhang et al., 2006). We have previously found that deactivation rates in GluR6 appear dominated by ligand dissociation (Zhang et al., 2008), which implies that Glu, but not KA, dissociates from D776K as quickly as it does from GluR6 WT. This emphasizes the fact that slower deactivation is not always associated with desensitization block, as with cyclothiazide action at AMPA receptors (Mitchell and Fleck, 2007), but also highlights an interesting ligand-specific difference in the phenotype of D776K.

Chaudhry et al. (2009) rightly underscored the difficulty of improving dimer packing by rational design; as with the original GluR3 L507Y mutant, our discovery of D776K was entirely

MOL #56598

serendipitous. If anything, the D776K mutation would have been expected to be destabilizing. Over the past ten years non-desensitizing AMPA-receptor mutants have provided a wealth of insights into the conformational requirements of both the desensitization and trafficking of AMPA receptors. As the first example of a kainate receptor subunit that is non-desensitizing in the absence of covalent cross-linkages, GluR6-D776K is closer in character to these AMPA-receptor mutants. It is to be hoped that, low expression notwithstanding, D776K may have the potential to fulfill an equivalent role for kainate receptors in the future.

#### **ACKNOWLEDGEMENTS**

We thank Kate Davis for technical assistance with mutagenesis and cell culture, and Sarah Lummis, Kerry Price and Andrew Thompson (University of Cambridge, UK) for providing facilities for and assistance with the oocyte recordings. We are also grateful to Steve Heinemann (Salk Institute, La Jolla, CA) for the gift of the rat GluR6(Q) cDNA and David Wyllie (University of Edinburgh, UK) for help with the fast perfusion system.

MOL #56598

## REFERENCES

- Armstrong N and Gouaux E (2000) Mechanisms for activation and antagonism of an AMPA-sensitive glutamate receptor: Crystal structures of the GluR2 ligand binding core. *Neuron* **28**:165-181.
- Bowie D (2002) External anions and cations distinguish between AMPA and kainate receptor gating mechanisms. *J Physiol* **539**:725-733.
- Bowie D, Garcia EP, Marshall J, Traynelis SF and Lange GD (2003) Allosteric regulation and spatial distribution of kainate receptors bound to ancillary proteins. *J Physiol* **547**:373-385.
- Chaudhry C, Weston MC, Schuck P, Rosenmund C and Mayer ML (2009) Stability of ligand-binding domain dimer assembly controls kainate receptor desensitization. *EMBO J* **28**:1518-1530.
- Clements JD, Feltz A, Sahara Y and Westbrook GL (1998) Activation kinetics of AMPA receptor channels reveal the number of functional agonist binding sites. *J Neurosci* **18**:119-127.
- Dam J and Schuck P (2004) Calculating sedimentation coefficient distributions by direct modeling of sedimentation velocity concentration profiles. *Methods Enzymol* **384**:185-212.
- Dingledine R, Borges K, Bowie D and Traynelis SF (1999) The glutamate receptor ion channels. *Pharmacol Rev* **51**:7-61.
- Fleck MW, Cornell E and Mah SJ (2003) Amino-acid residues involved in glutamate receptor 6 kainate receptor gating and desensitization. *J Neurosci* **23**:1219-1227.
- Gouaux E (2004) Structure and function of AMPA receptors. *J Physiol* **554**:249-253.
- Greger IH, Khatri L, Kong X and Ziff EB (2003) AMPA receptor tetramerization is mediated by Q/R editing. *Neuron* **40**:763-774.

MOL #56598

- Heckmann M, Bufler J, Franke C and Dudel J (1996) Kinetics of homomeric GluR6 glutamate receptor channels. *Biophys J* **71**:1743-1750.
- Horning MS and Mayer ML (2004) Regulation of AMPA receptor gating by ligand binding core dimers. *Neuron* **41**:379-388.
- Jatzke C, Watanabe J and Wollmuth LP (2002) Voltage and concentration dependence of Ca(2+) permeability in recombinant glutamate receptor subtypes. *J Physiol* **538**:25-39.
- Laue TM, Shah BD, Ridgeway TM and Pelletier SL (1992) Computer-aided interpretation of analytical sedimentation data for proteins, in *Analytical Ultracentrifugation in Biochemistry and Polymer Sciences* (Harding SE, Rowe AJ and Horton JC eds) pp 90-125, Royal Society for Chemistry, Cambridge, UK.
- Mayer ML (2005) Crystal structures of the GluR5 and GluR6 ligand binding cores: molecular mechanisms underlying kainate receptor selectivity. *Neuron* **45**:539-552.
- Mayer ML (2006) Glutamate receptors at atomic resolution. *Nature* **440**:456-462.
- Mitchell NA and Fleck MW (2007) Targeting AMPA receptor gating processes with allosteric modulators and mutations. *Biophys J* **92**:2392-2402.
- Nanao MH, Green T, Stern-Bach Y, Heinemann SF and Choe S (2005) Structure of the kainate receptor subunit GluR6 agonist-binding domain complexed with domoic acid. *Proc Natl Acad Sci USA* **102**:1708-1713.
- Ozawa S, Kamiya H and Tsuzuki K (1998) Glutamate receptors in the mammalian central nervous system. *Prog Neurobiol* **54**:581-618.
- Paternain AV, Cohen A, Stern-Bach Y and Lerma J (2003) A role for extracellular Na<sup>+</sup> in the channel gating of native and recombinant kainate receptors. *J Neurosci* **23**:8641-8648.
- Pei W, Ritz M, McCarthy M, Huang Z and Niu L (2007) Receptor occupancy and channel-opening kinetics: a study of GLUR1 L497Y AMPA receptor. *J Biol Chem* **282**:22731-22736.



MOL #56598

Penn AC, Williams SR and Greger IH (2008) Gating motions underlie AMPA receptor secretion from the endoplasmic reticulum. *EMBO J* **27**:3056-3068.

Plested AJ and Mayer ML (2007) Structure and mechanism of kainate receptor modulation by anions. *Neuron* **53**:829-841.

Plested AJ, Vijayan R, Biggin PC and Mayer ML (2008) Molecular basis of kainate receptor modulation by sodium. *Neuron* **58**:720-735.

Priel A, Selak S, Lerma J and Stern-Bach Y (2006) Block of kainate receptor desensitization uncovers a key trafficking checkpoint. *Neuron* **52**:1037-1046.

Robert A and Howe JR (2003) How AMPA receptor desensitization depends on receptor occupancy. *J Neurosci* **23**:847-858.

Rosenmund C, Stern-Bach Y and Stevens CF (1998) The tetrameric structure of a glutamate receptor channel. *Science* **280**:1596-1599.

Stafford WF and Sherwood PJ (2004) Analysis of heterologous interacting systems by sedimentation velocity: Curve fitting algorithms for estimation of sedimentation coefficients, equilibrium and kinetic constants. *Biophys Chem* **108**:231-243.

Stern-Bach Y, Russo S, Neuman M and Rosenmund C (1998) A point mutation in the glutamate binding site blocks desensitization of AMPA receptors. *Neuron* **21**:907-918.

Sun Y, Olson R, Horning M, Armstrong N, Mayer M and Gouaux E (2002) Mechanism of glutamate receptor desensitization. *Nature* **417**:245-253.

Thompson AJ and Lummis SC (2008) Antimalarial drugs inhibit human 5-HT(3) and GABA(A) but not GABA(C) receptors. *Br J Pharmacol* **153**:1686-1696.

Weston MC, Schuck P, Ghosal A, Rosenmund C and Mayer ML (2006) Conformational restriction blocks glutamate receptor desensitization. *Nat Struct Mol Biol* **13**:1120-1127.

MOL #56598

Wong AY, Fay AM and Bowie D (2006) External ions are coactivators of kainate receptors. *J Neurosci* **26**:5750-5755.

Wong AY, MacLean DM and Bowie D (2007) Na<sup>+</sup>/Cl<sup>-</sup> Dipole Couples Agonist Binding to Kainate Receptor Activation. *J Neurosci* **27**:6800-6809.

Zhang Y, Nayeem N and Green T (2008) Mutations to the kainate receptor subunit GluR6 binding pocket that selectively affect domoate binding. *Mol Pharmacol* **74**:1163-1169.

Zhang Y, Nayeem N, Nanao MH and Green T (2006) Interface interactions modulating desensitization of the kainate-selective ionotropic glutamate receptor subunit GluR6. *J Neurosci* **26**:10033-10042.

MOL #56598

## FOOTNOTES

This work was supported by the UK Medical Research Council [Grant G0200084].

Reprint requests should be sent to Dr T. Green, Department of Pharmacology, School of Biomedical Sciences, University of Liverpool, Ashton Street, Liverpool L69 3GE, UK. e-mail: [tpgreen@liv.ac.uk](mailto:tpgreen@liv.ac.uk)

<sup>1</sup>N.N. and Y.Z. contributed equally to this work.

<sup>2</sup>Current affiliation: Department of Physiology & Pharmacology, University of Bristol, University Walk, Bristol, BS8 1TD, UK.

MOL #56598

## LEGENDS FOR FIGURES

**Figure 1.** Ionic interactions at the apex of kainate S1S2 domain dimers.

**A**, The GluR6 S1S2-domoate dimer interface (Nanao et al., 2005) viewed from the side. Protomers B and D (gold & blue respectively, cartoon representation) are shown with domoate (black) and the apical residues Glu524 (yellow), Lys531 (gray), Arg775 (green) and Asp776 (magenta), all in space-fill representation. Nitrogens and oxygens are colored blue and red respectively. **B**, Closer view of apical cluster, from the top (left panel) and side (right panel; looking through protomer B) of the S1S2 dimer. Residues are colored as in **A**. For clarity, only selected parts of the protomer B main chain (partially transparent cartoon) are shown in the right panel. Polar contacts are indicated (dotted gray lines). **C**, Equivalent views of the GluR5 S1S2-KA complex (Plested et al., 2008), viewed as in **B** (protomer A, pink; protomer B, light green). The GluR5 homologs of Glu524, Lys531, Arg775 and Asp776 (Glu539, Lys546, Arg790 & Asp791) are shown, as are the chloride (green) and sodium (blue) ions.

**Figure 2.** Varied effects of charge exchanges to apical GluR6 residues.

**A**, Representative current responses recorded from HEK cells transiently transfected with the E524K-K531E double mutant and the R775D and K531E single mutants. Applications (100 ms) of Glu (3 mM, black line above trace) and KA (1 mM, gray line above trace) are shown, along with normalized GluR6 WT traces (gray dotted; top & bottom mutants only), to allow comparison of desensitization rates. **B**, Representative responses to applications of Glu and KA recorded from cells expressing GluR6 D776K. Traces from 4 s agonist applications are shown to illustrate the almost complete lack of desensitization. **C**, Traces from brief (1 ms) agonist applications to illustrate peak decay rates from D776K (black traces), compared to GluR6 WT (normalized traces; gray, dotted).

MOL #56598

**Figure 3.** D776K oligomerization, surface expression and trafficking.

**A**, Oligomerization differences between GluR6 WT and D776K S1S2 domains. Recombinant S1S2 domains were separated by gel filtration and the protein visualized by Coomassie blue staining following SDS-PAGE (top panel). The D776K mutant resolved in earlier fractions, indicating a higher apparent molecular weight. Protein-containing fractions were pooled, concentrated, and separated by Blue-Native PAGE stain using silver stain (lower panel). Monomers (open arrow) and dimers (gray arrow) were apparent in both samples, while higher-order multimers (black arrow) were also present in D776K S1S2. **B**, Quantification of the GluR6 WT & D776K S1S2 domain monomer:dimer equilibrium by sedimentation equilibrium. Absorbance data collected at 14,000 rpm (open circles, top panel) are shown for one channel for the WT (left) and D776K mutant (right), together with global fits obtained using fixed molecular-weight, single-species (dashed line) or a monomer:dimer equilibrium (solid line, mutant only) models. The residuals (observed-calculated) associated with each fit are shown in the bottom panels for the single-species (open circles) and monomer:dimer equilibrium (filled squares). The data indicate that there is a significant dimer component for D776K but not GluR6 WT, under the conditions tested. **C**, Immunoblots (with anti-GluR6/7) showing relative total (Tot) and surface (Sur) expression of GluR6 WT, E524K and D776K determined by surface biotinylation (see *Materials & Methods*). Surface labeling of D776K was extremely weak or absent (n=3). The positions of molecular weight markers are indicated. **D**, Immunoblot showing the results of enzymatic deglycosylation of GluR6 WT and D776K using Endo H and PNGase F, carried out as described in the *Materials & Methods*. Control samples were treated as for PNGase F but without enzyme. The sizes of immature (Endo H sensitive; black arrow), mature (Endo H insensitive;

MOL #56598

gray arrow) and unglycosylated (open arrow) GluR6 are indicated (right), as are the positions of molecular weight markers (left). No mature glycosylation was evident in D776K samples (n=3).

**Figure 4.** Anion and cation sensitivity of D776K.

Scatter-plot showing responses to Glu (10mM) from *Xenopus* oocytes expressing the GluR6 D776K mutant, recorded in buffers where either the cation or anion was exchanged. Responses were normalized to control responses (in NaCl), recorded before and after each test response. Scatter for control NaCl responses reflects the variability observed in individual oocytes. Data were collected from five oocytes. Dotted lines show the means for each group, with errors (SEM) in gray. Responses in all four test buffers differed significantly from the NaCl control ( $P < 0.001$ ). For comparison, normalized response levels from ConA-treated oocytes expressing GluR6 WT are indicated by arrows for each ion condition.

MOL #56598

**Table 1.** Desensitization kinetics of GluR6 mutants.

Mutant	Glu				KA			
	$I_{\text{peak}}$ (nA)	$\tau_{\text{Des}}$ (ms)	%des	( <i>n</i> )	$I_{\text{KA/Glu}}$	$\tau_{\text{Des}}$ (ms)	%des	( <i>n</i> )
Wild type	6.8±0.9	5.0±0.2	99.7±0.1	(21)	0.62±0.05	3.9±0.2	99.4±0.1	(12)
E524 K	N.R.	-	-	(10)	N.R.	-	-	(10)
K531 E	5.6±0.7	<b>9.1±0.6***</b>	99.8±0.1	(11)	<b>1.03±0.03***</b>	<b>34.5±3.9***</b> (1s)	98.4±0.7 (1s)	(13)
E524 K K531 E	0.03±0.01	<sup>a</sup> 1.3±0.2	100	(11)	<sup>b</sup> N.D.	<sup>c</sup> 1.4±0.1	100	(11)
R775 D	0.01±0.003	N.D.	N.D.	(11)	<sup>d</sup> N.D.	N.D.	N.D.	(11)
D776 K	0.83±0.3	N.D.	<sup>e</sup> <b>9.5±1.6***</b> (4s)	(30)	<b>0.86±0.03**</b>	N.D.	<sup>f</sup> <b>10.3±1.2**</b> (4s)	(24)
R775 D D776 R	N.R.	-	-	(7)	N.R.	-	-	(7)

$I_{\text{peak}}$ ,  $\tau_{\text{Des}}$ , and %des and  $I_{\text{KA/Glu}}$  are peak currents, desensitization time-constant, percentage desensitization and relative KA efficacy respectively (mean±S.E.M. for *n* determinations), recorded from transiently-transfected HEK cells. Kinetics were determined from 100 ms agonist applications except where indicated in brackets. N.R. is no response. N.D. is not determined. Boldface type indicates significant differences comparing  $\tau_{\text{Des}}$ , %des and  $I_{\text{KA/Glu}}$  values with those of GluR6 WT (not tested for E524K-K531E or R775D mutants owing to small current sizes); \*\*  $P < 0.01$ ; \*\*\*  $P < 0.001$ . <sup>a</sup>*n*=4; <sup>b</sup>mean response to KA was 0.12±0.05 nA; <sup>c</sup>*n*=5; <sup>d</sup>mean response to KA 0.01±0.004 nA; <sup>e</sup>*n*=21; <sup>f</sup>*n*=20.

MOL #56598

**Table 2.** Deactivation kinetics of GluR6 mutants.

Mutant	Glu		KA	
	$\tau_{Dec-1ms}$	$\tau_{Dec-SS}$	$\tau_{Dec-1ms}$	$\tau_{Dec-SS}$
Wild type	3.9±0.2 (17)	10.8±2.4 (6)	4.4±0.2 (17)	127±32 (5)
“Quad”	<b>37±2.2***</b> (4)	<b>93±16***</b> (12)	N.D.	1,050±170 (12)
K531 E	2.5±0.3 (10)	N.D.	<b>14.2±1.0***</b> (10)	N.D.
D776 K	3.9±0.3 (18)	<b>5.7±0.4*</b> (25)	<b>47±2.3***</b> (18)	57±3.9 (21)

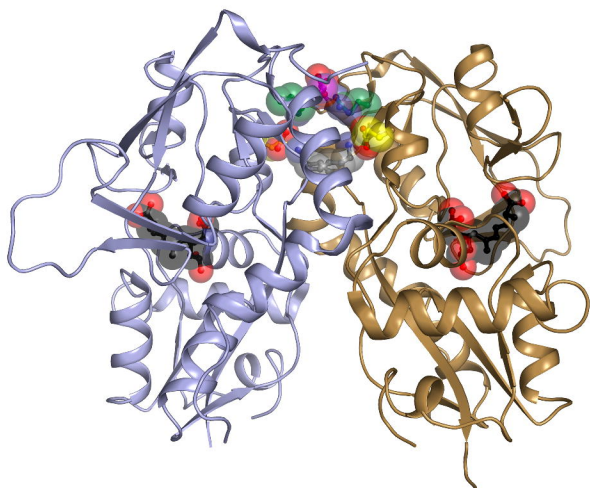
$\tau_{Dec-1ms}$  and  $\tau_{Dec-SS}$  are the deactivation rate from peak and deactivation rate from steady state, determined as described in the *Materials & Methods*. Values are shown mean±S.E.M. for (*n*) determinations. Boldface type indicates significant differences comparing  $\tau_{Dec-1ms}$  or  $\tau_{Dec-SS}$  values with those of GluR6 WT; \*  $P < 0.05$ , \*\*\*  $P < 0.001$ . N.D. is not determined. “Quad” is the GluR6 K525E/K696R/I780L/Q784K mutant characterized in Zhang et al. (2006).



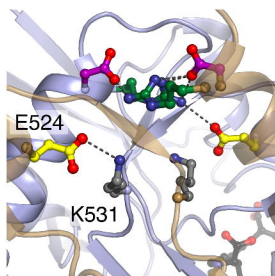
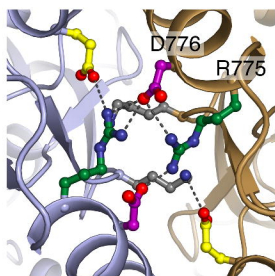
Fig. 1

A

GluR6 S1S2-Dom



B



C

GluR5 S1S2-KA

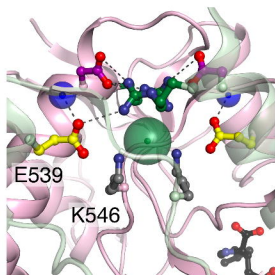
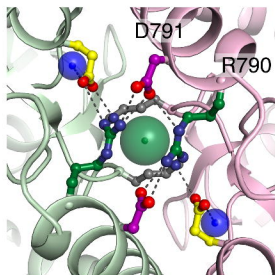
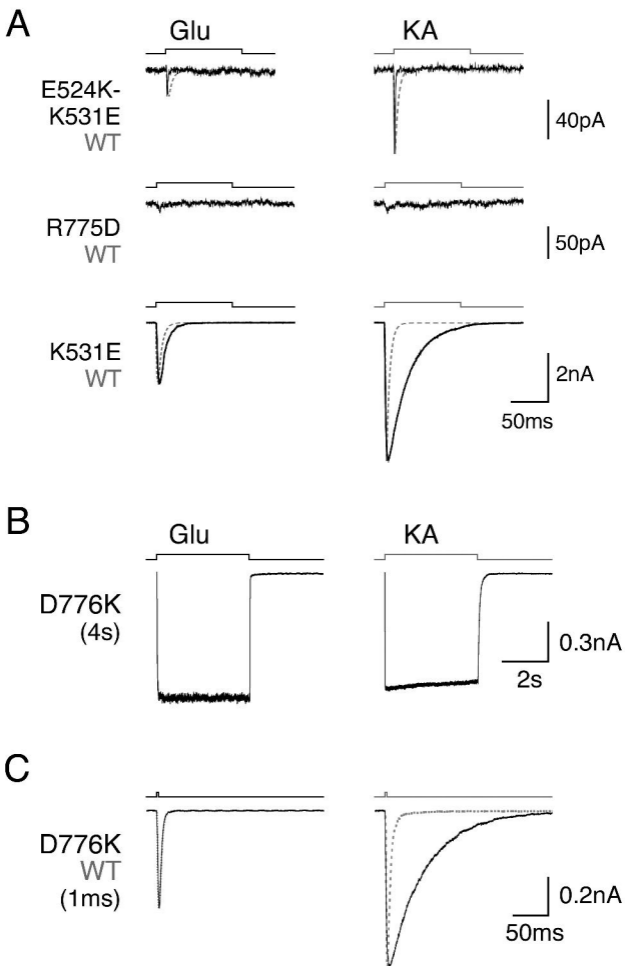


Fig. 2



**Fig. 3**

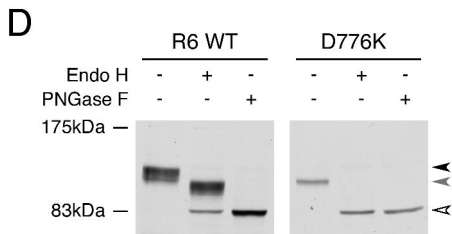
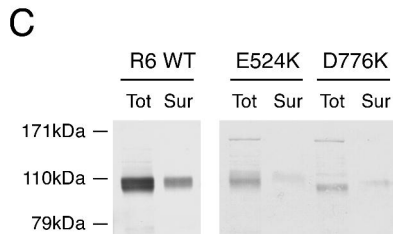
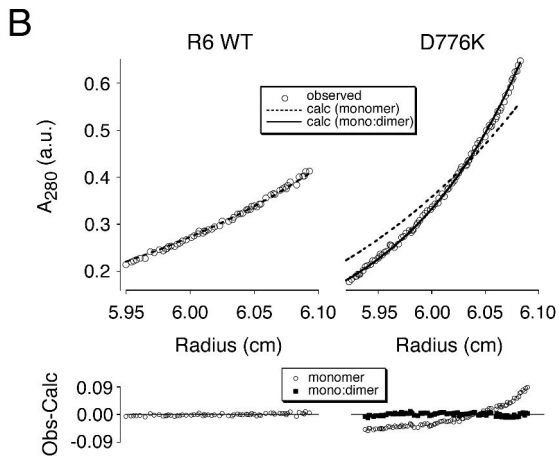
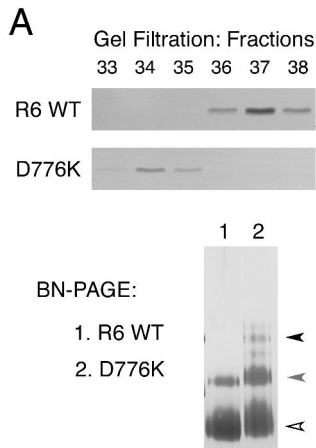


Fig. 4

